ELECTRONIC SUPPLEMENTARY INFORMATION

Mode-specific quasi-classical dynamics of the $F^- + SiH_3Cl$ system

Attila Á. Dékány, Balázs J. Molnár and Gábor Czakó*

MTA-SZTE Lendület "Momentum" Computational Reaction Dynamics Research Group, Interdisciplinary Excellence Centre and Department of Physical Chemistry and Materials Science, Institute of Chemistry, University of Szeged, Rerrich Béla tér 1, Szeged H-6720, Hungary

* E-mail: gczako@chem.u-szeged.hu

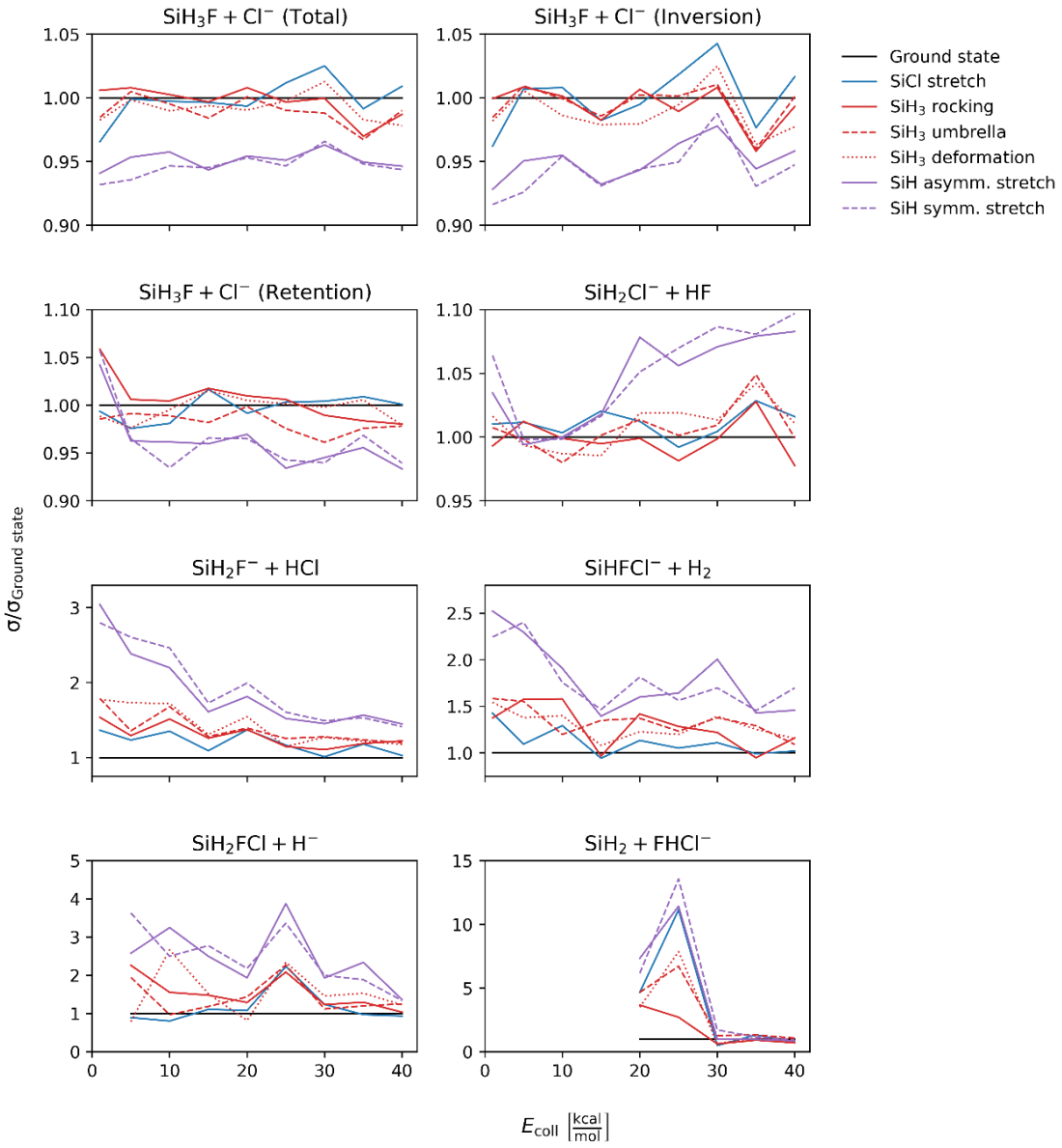

Figure S1. Mode-specific integral cross section ratios ($\sigma/\sigma_{\text{Ground state}}$) of the $F^- + SiH_3Cl(v_k = 0, 1)$ reactions as a function of collision energy obtained by analyzing the first half of the trajectories.

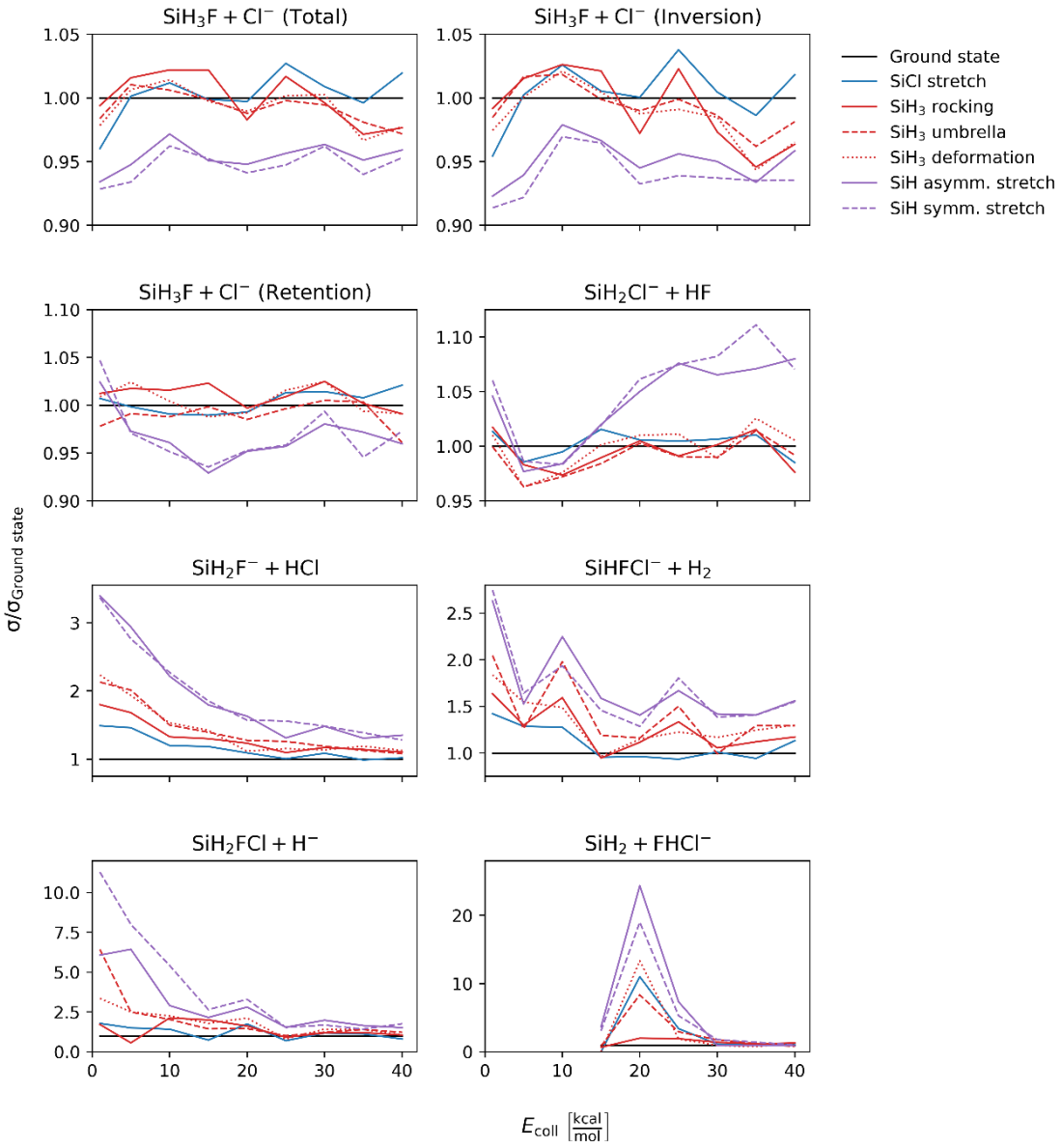

Figure S2. Mode-specific integral cross section ratios ($\sigma/\sigma_{\text{Ground state}}$) of the $F^- + SiH_3Cl(v_k = 0, 1)$ reactions as a function of collision energy obtained by analyzing the second half of the trajectories.

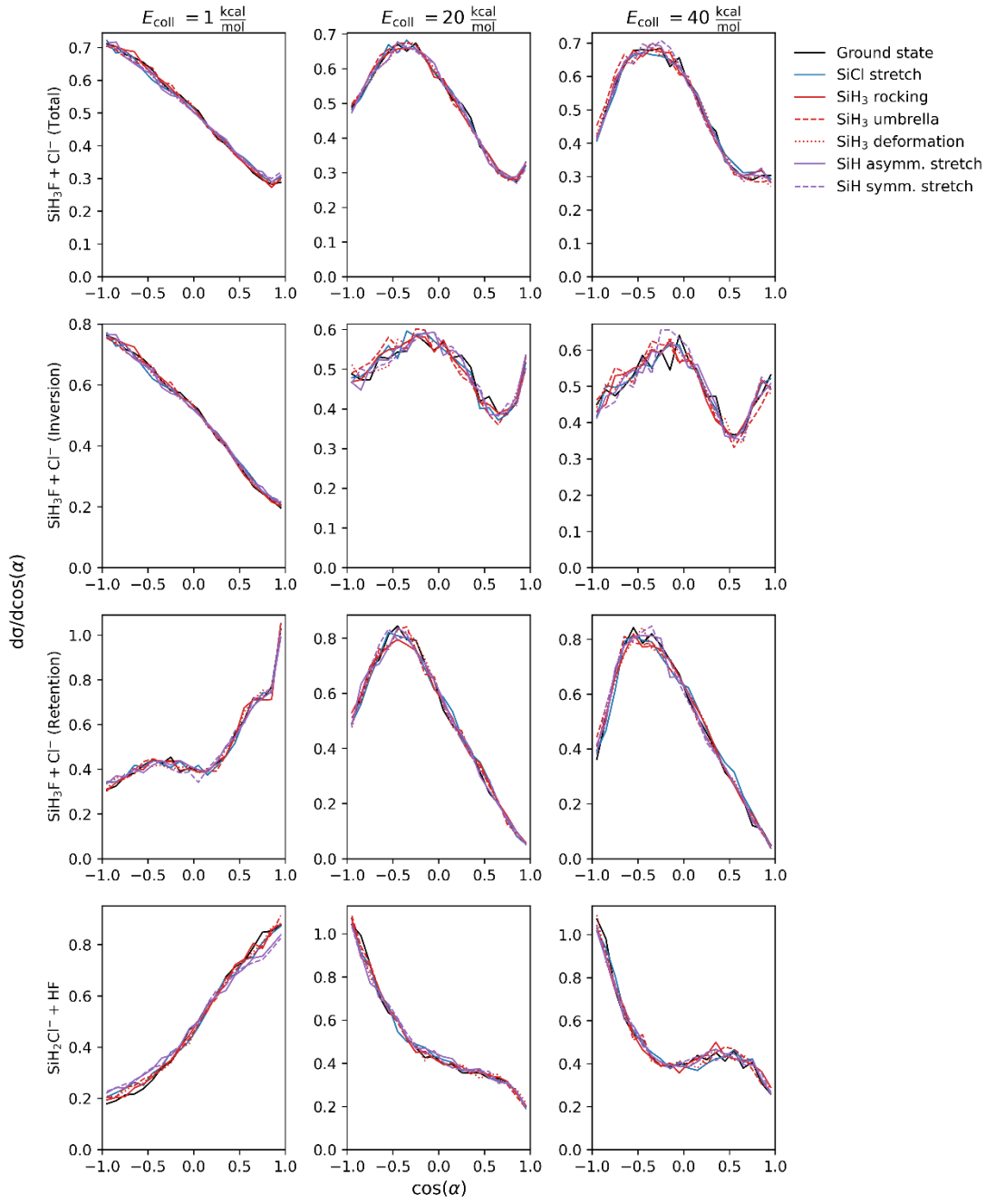

Figure S3. Mode-specific initial attack angle distributions of the F^- + $SiH_3Cl(v_k = 0, 1)$ chloride-ion substitution (divided into inversion and retention channels) and proton-abstraction reactions at E_{coll} = 1, 20 and 40 kcal/mol.

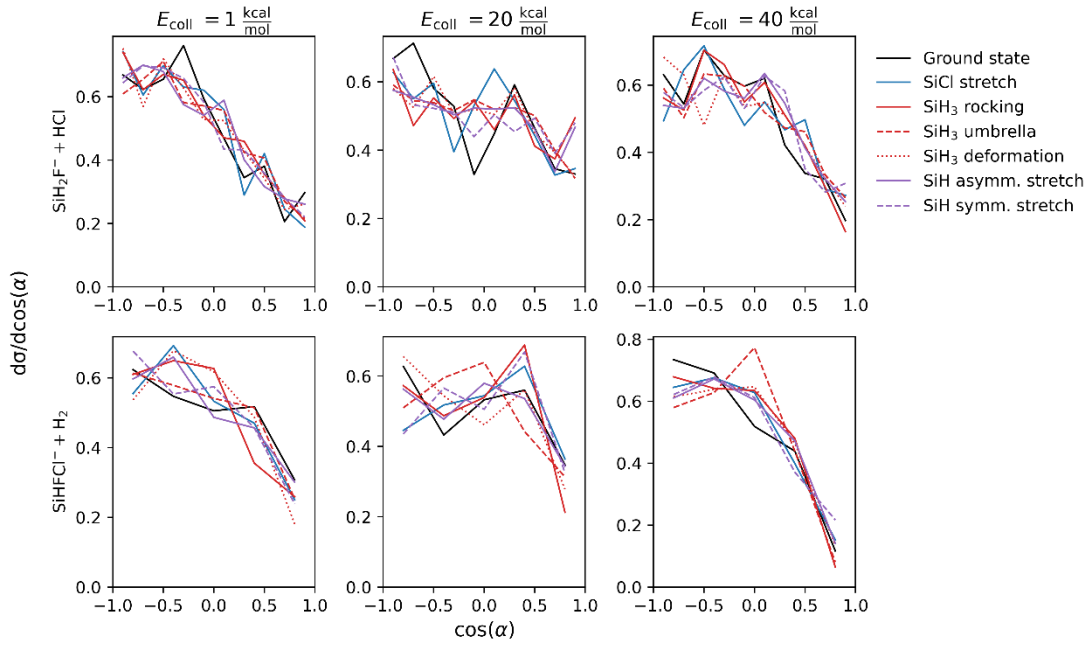

Figure S4. Mode-specific initial attack angle distributions of the F^- + $SiH_3Cl(v_k = 0, 1)$ hydrogen-chloride and molecular-hydrogen production reactions at E_{coll} = 1, 20 and 40 kcal/mol.

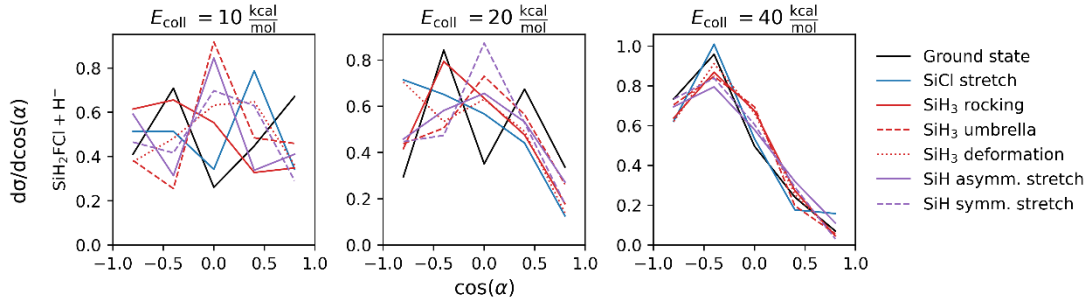

Figure S5. Mode-specific initial attack angle distributions of the F^- + $SiH_3Cl(v_k = 0, 1)$ hydride-ion substitution at E_{coll} = 10, 20 and 40 kcal/mol.

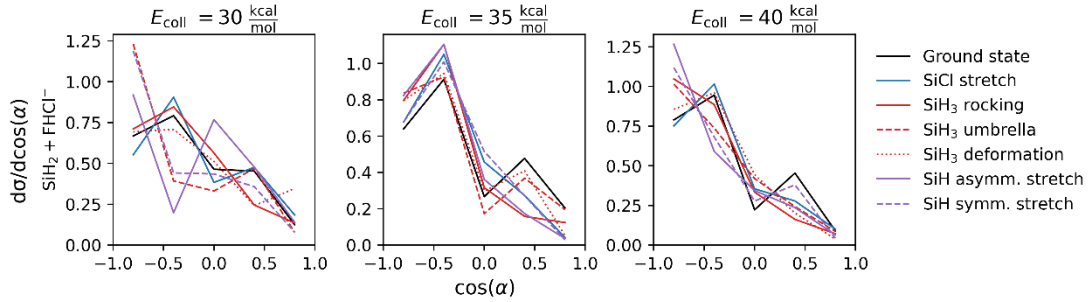

Figure S6. Mode-specific initial attack angle distributions of the F^- + $SiH_3Cl(v_k = 0, 1)$ bihalide-ion production reaction at E_{coll} = 30, 35 and 40 kcal/mol.

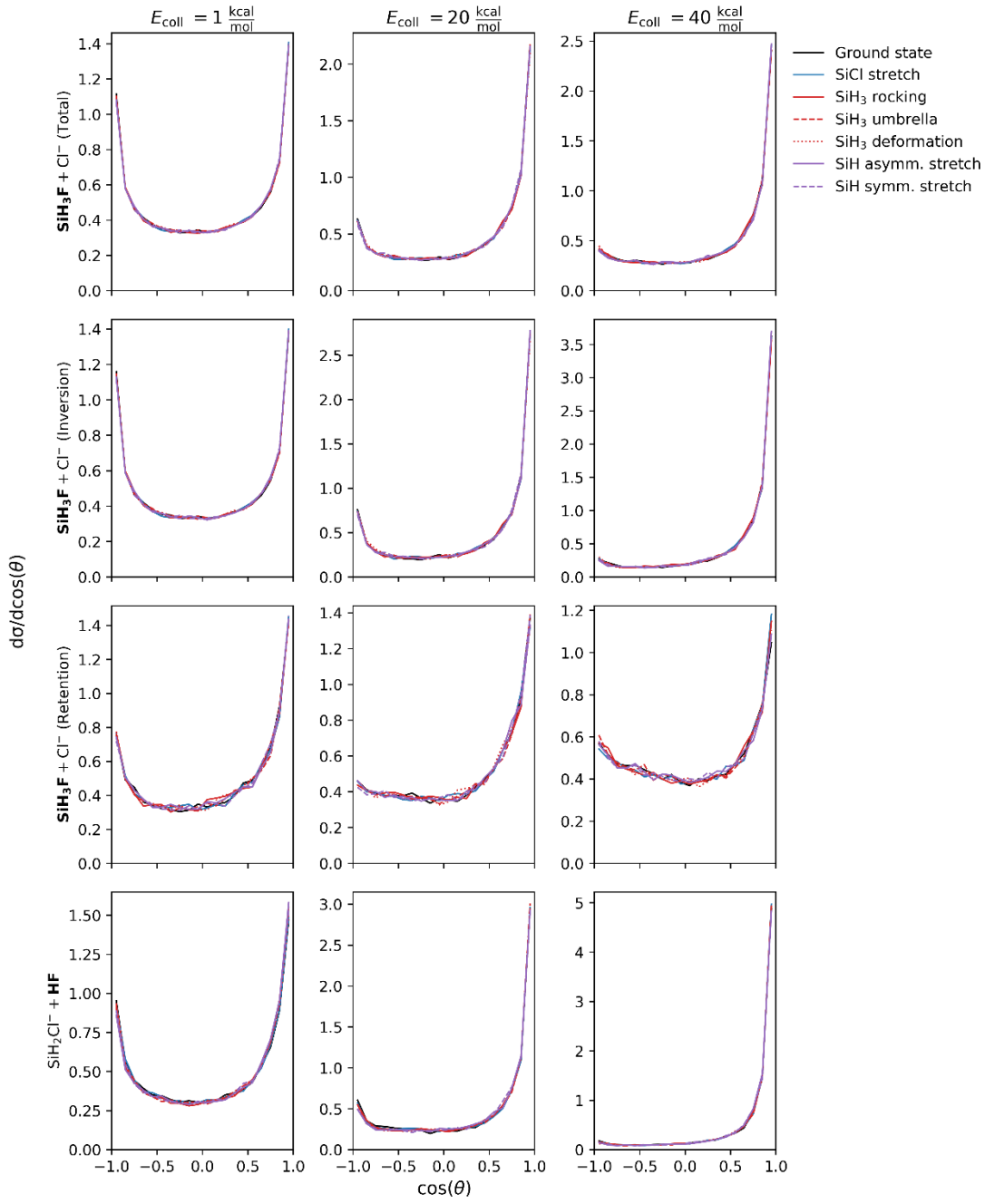

Figure S7. Mode-specific scattering angle distributions of the F^- + $SiH_3Cl(v_k = 0, 1)$ chloride-ion substitution (divided into inversion and retention channels) and proton-abstraction reactions at E_{coll} = 1, 20 and 40 kcal/mol.

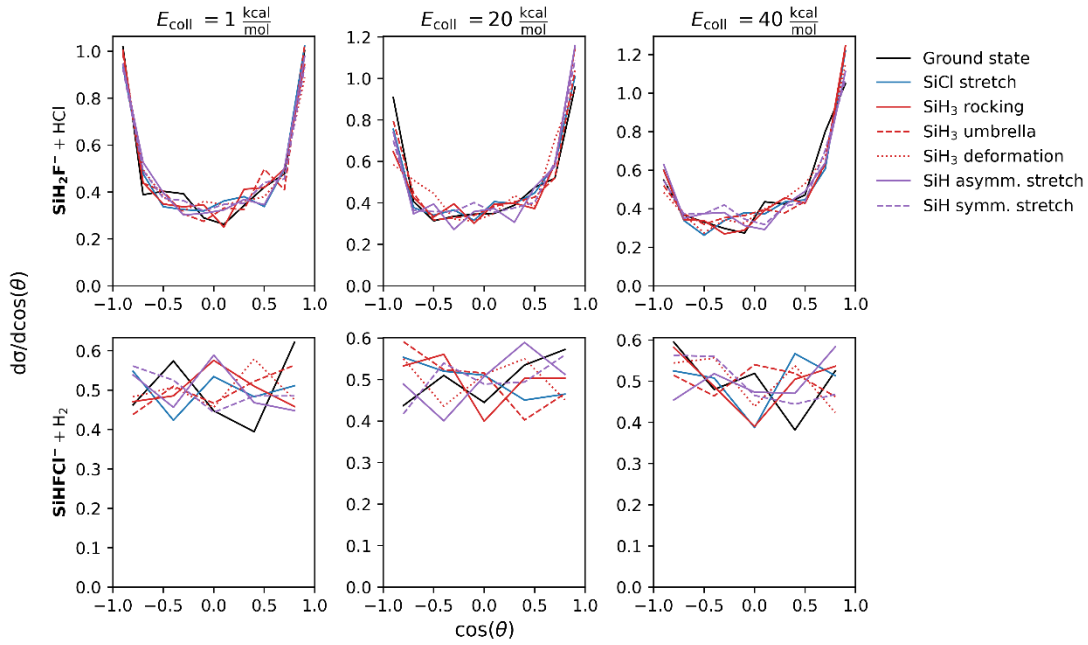

Figure S8. Mode-specific scattering angle distributions of the F^- + $SiH_3Cl(v_k = 0, 1)$ hydrogen-chloride and molecular-hydrogen production reactions at E_{coll} = 1, 20 and 40 kcal/mol.

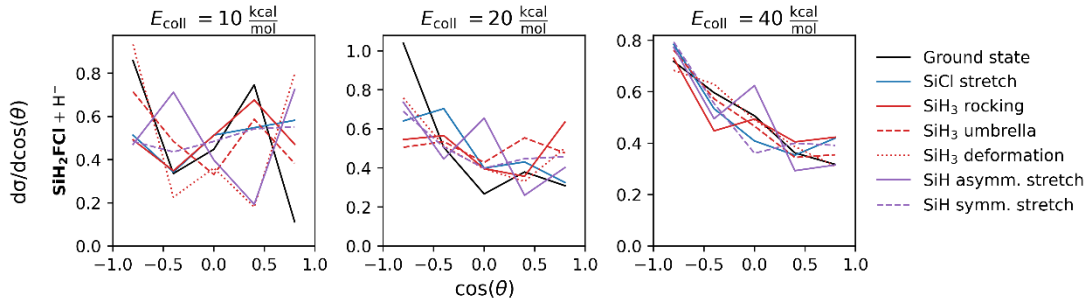

Figure S9. Mode-specific scattering angle distributions of the F^- + $SiH_3Cl(v_k = 0, 1)$ hydride-ion substitution at E_{coll} = 10, 20 and 40 kcal/mol.

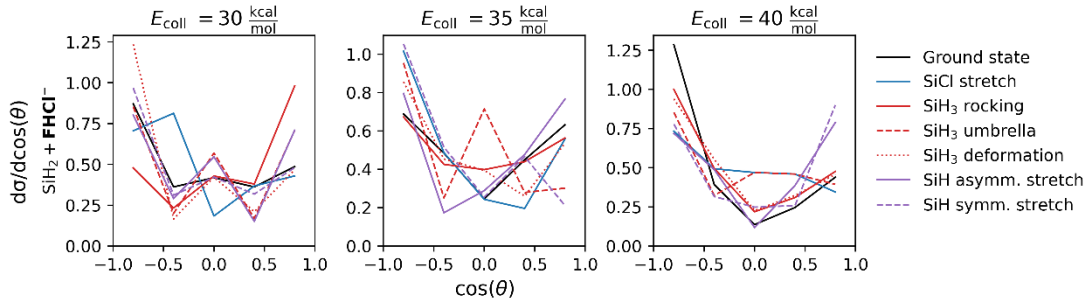

Figure S10. Mode-specific scattering angle distributions of the F^- + $SiH_3Cl(v_k = 0, 1)$ bihalide-ion production reaction at E_{coll} = 30, 35 and 40 kcal/mol.

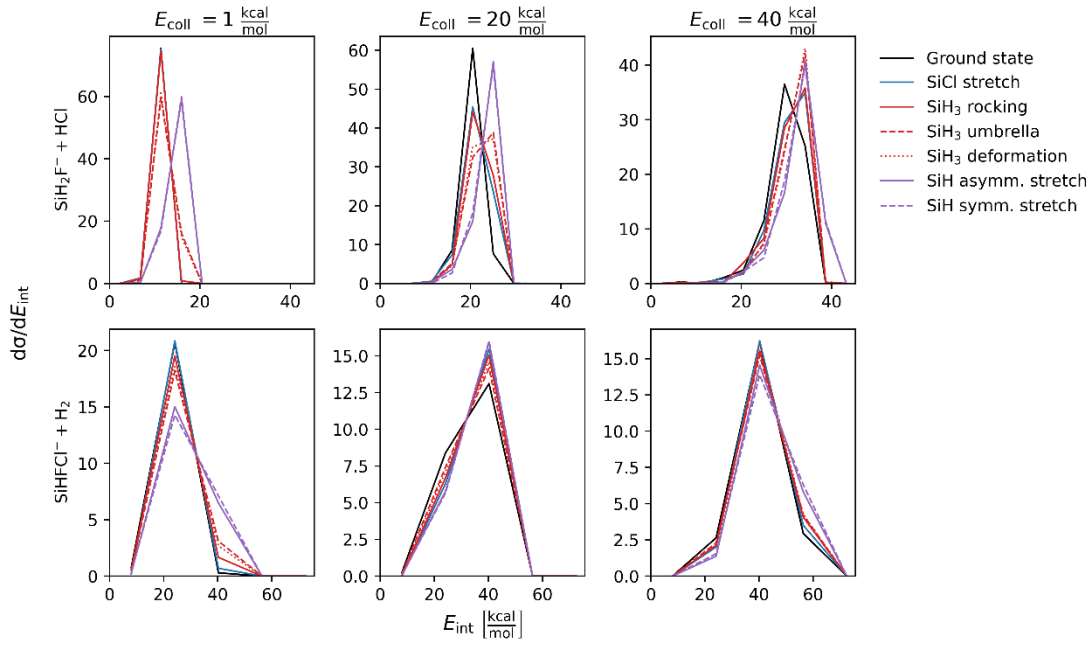

Figure S11. Mode-specific internal energy distributions of the F^- + $SiH_3Cl(v_k = 0, 1)$ hydrogen-chloride and molecular-hydrogen production reactions at E_{coll} = 1, 20 and 40 kcal/mol.

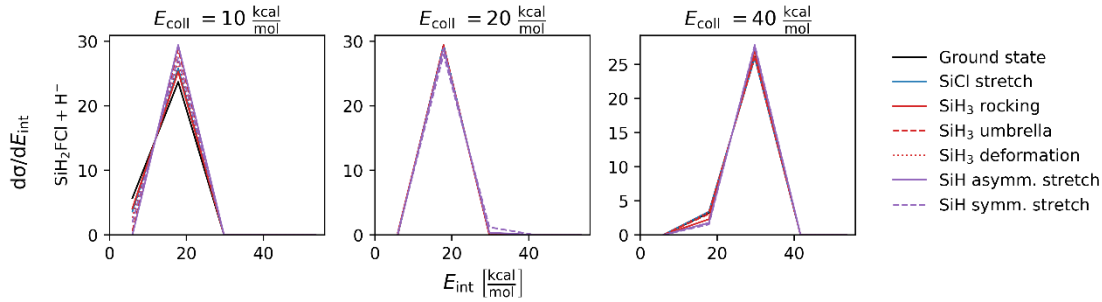

Figure S12. Mode-specific internal energy distributions of the F^- + $SiH_3Cl(v_k = 0, 1)$ hydride-ion substitution at E_{coll} = 10, 20 and 40 kcal/mol.

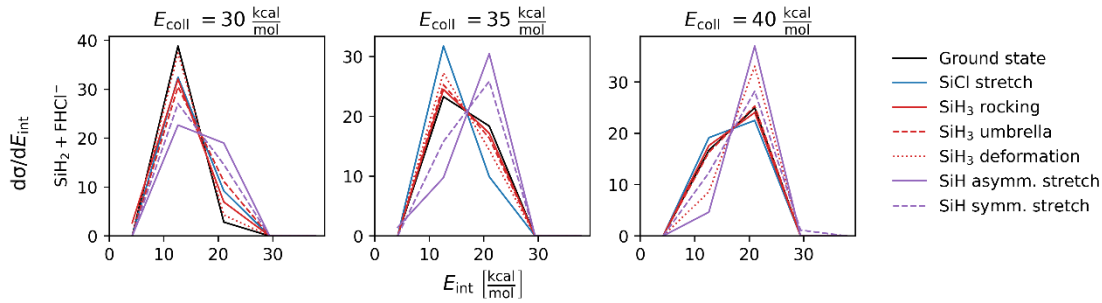

Figure S13. Mode-specific internal energy distributions of the F^- + $SiH_3Cl(v_k = 0, 1)$ bihalide-ion production reaction at E_{coll} = 30, 35 and 40 kcal/mol.

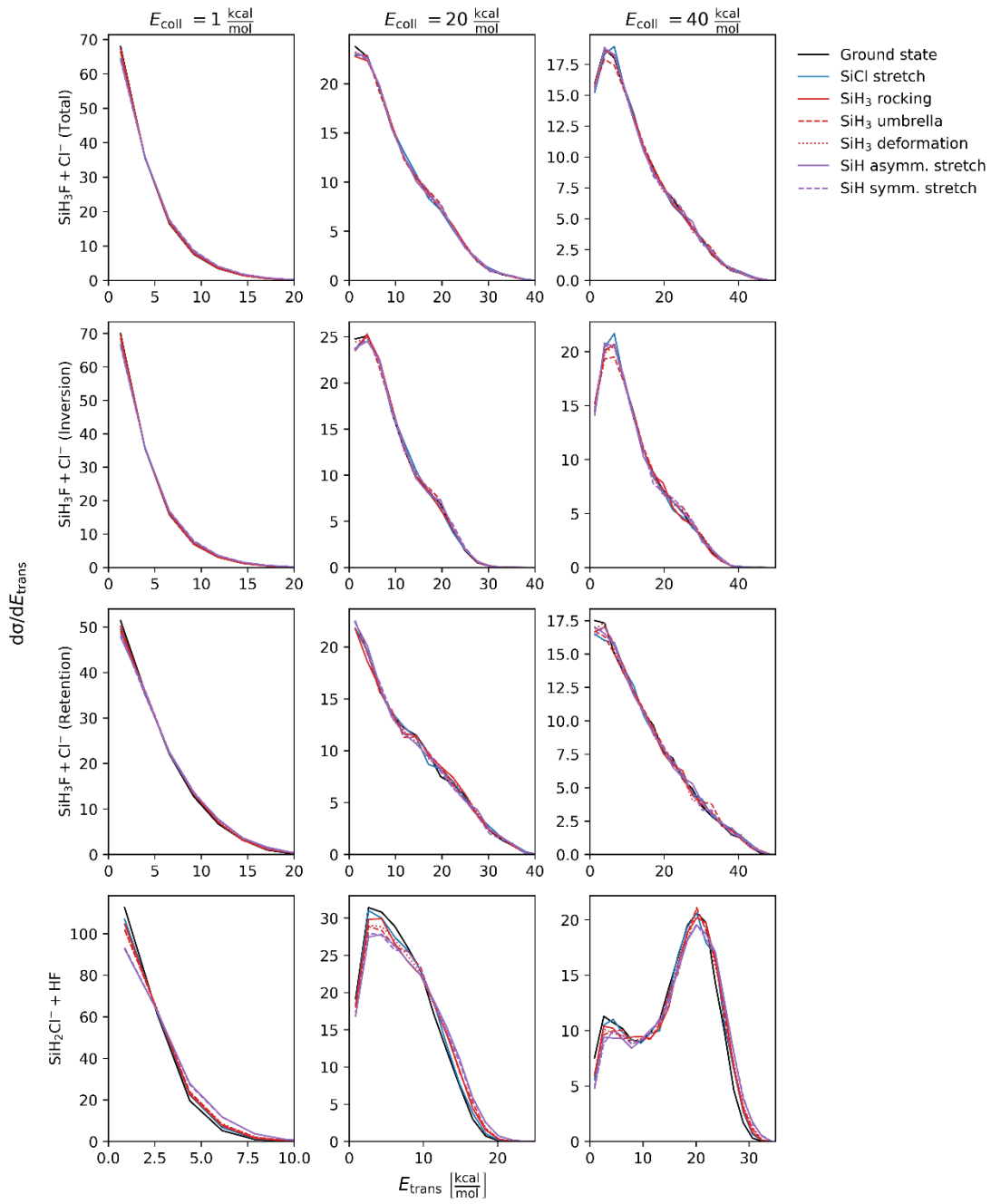

Figure S14. Mode-specific translational energy distributions of the F^- + $SiH_3Cl(v_k = 0, 1)$ chloride-ion substitution (divided into inversion and retention channels) and proton-abstraction reactions at E_{coll} = 1, 20 and 40 kcal/mol.

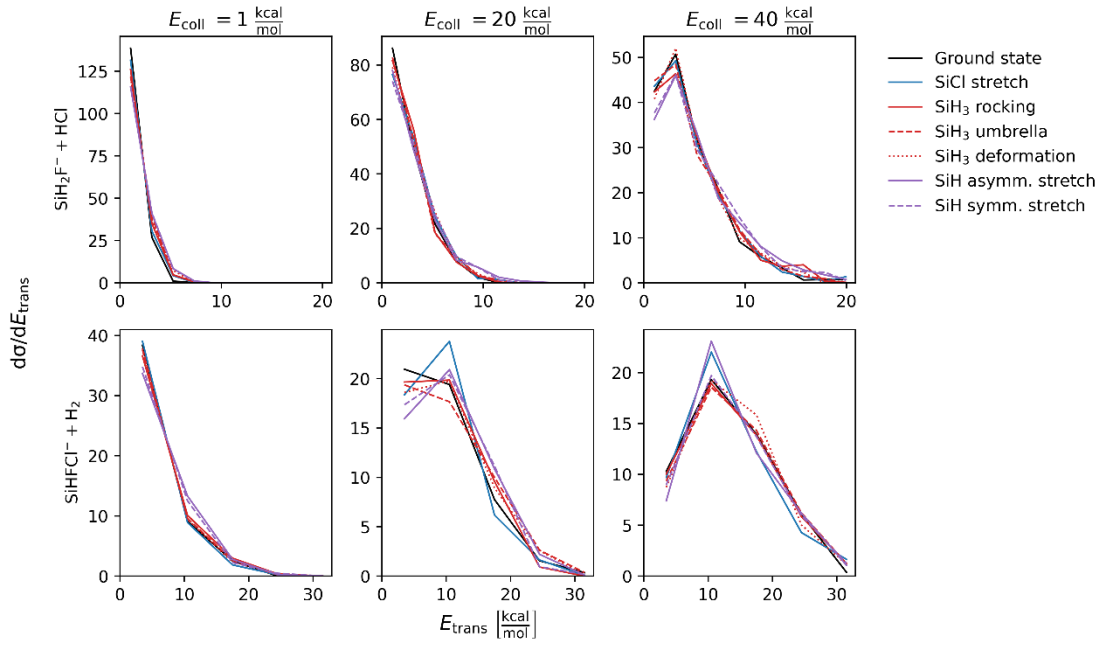

Figure S15. Mode-specific translational energy distributions of the F^- + $SiH_3Cl(v_k$ = 0, 1) hydrogen-chloride and molecular-hydrogen production reactions at E_{coll} = 1, 20 and 40 kcal/mol.

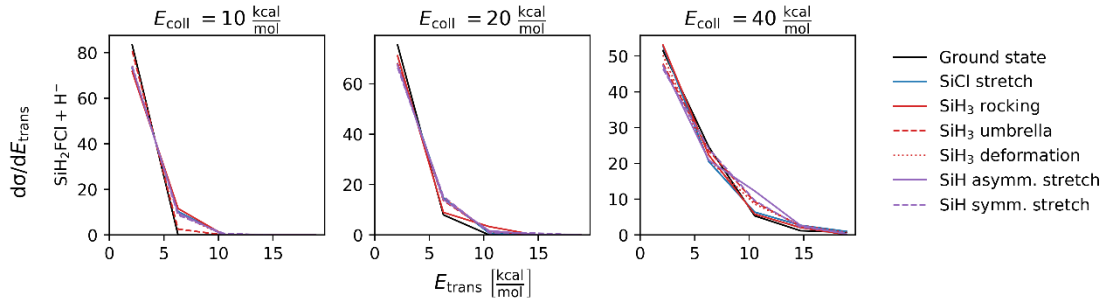

Figure S16. Mode-specific translational energy distributions of the F^- + $SiH_3Cl(v_k$ = 0, 1) hydride-ion substitution at E_{coll} = 10, 20 and 40 kcal/mol.

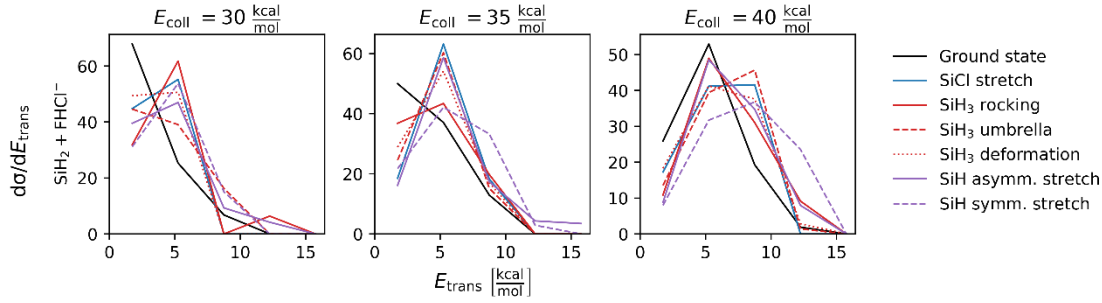

Figure S17. Mode-specific translational energy distributions of the F^- + $SiH_3Cl(v_k$ = 0, 1) bihalide-ion production reaction at E_{coll} = 30, 35 and 40 kcal/mol.

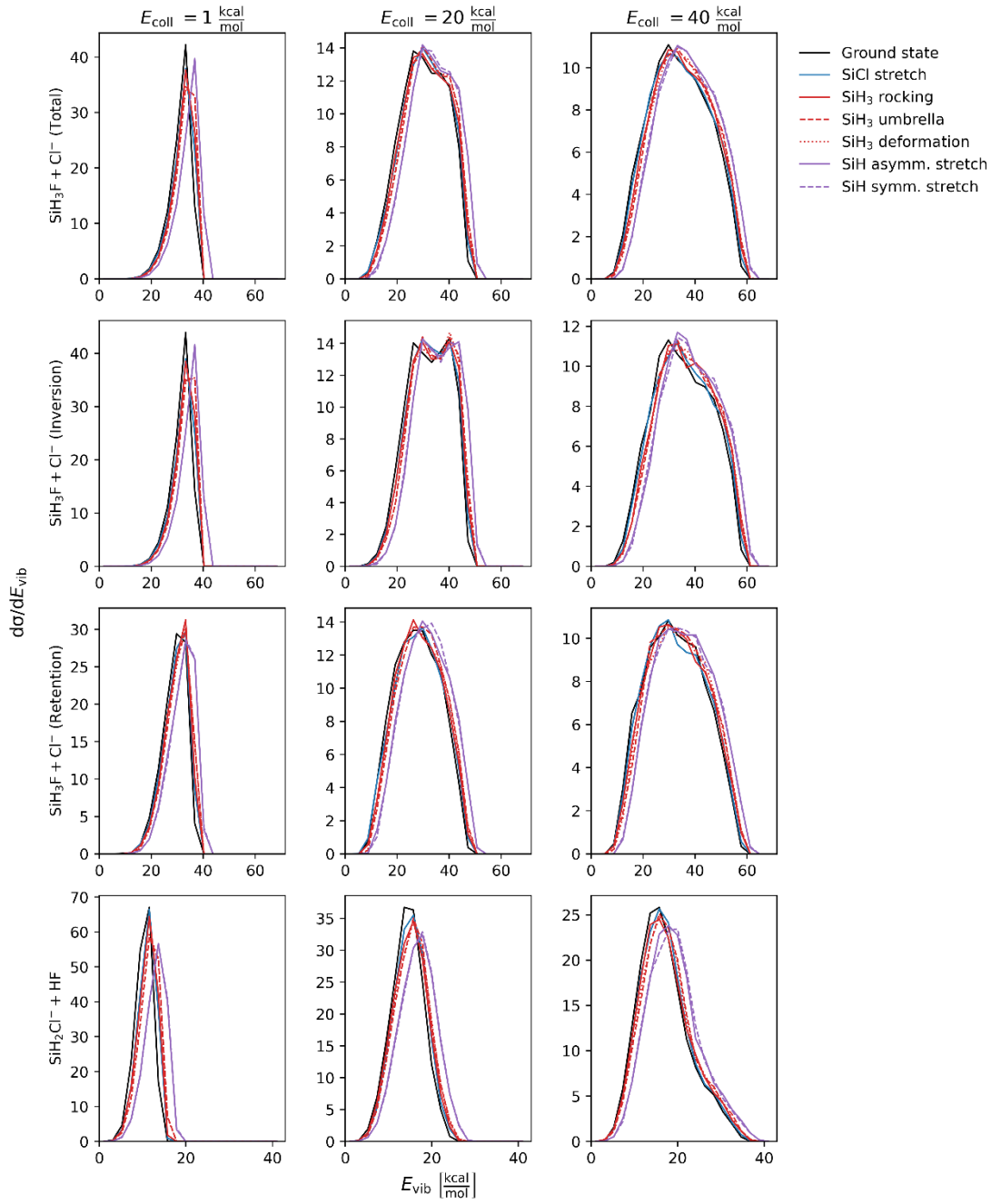

Figure S18. Mode-specific vibrational energy distributions of the F^- + $SiH_3Cl(\nu_k$ = 0, 1) chloride-ion substitution (divided into inversion and retention channels) and proton-abstraction reactions at E_{coll} = 1, 20 and 40 kcal/mol.

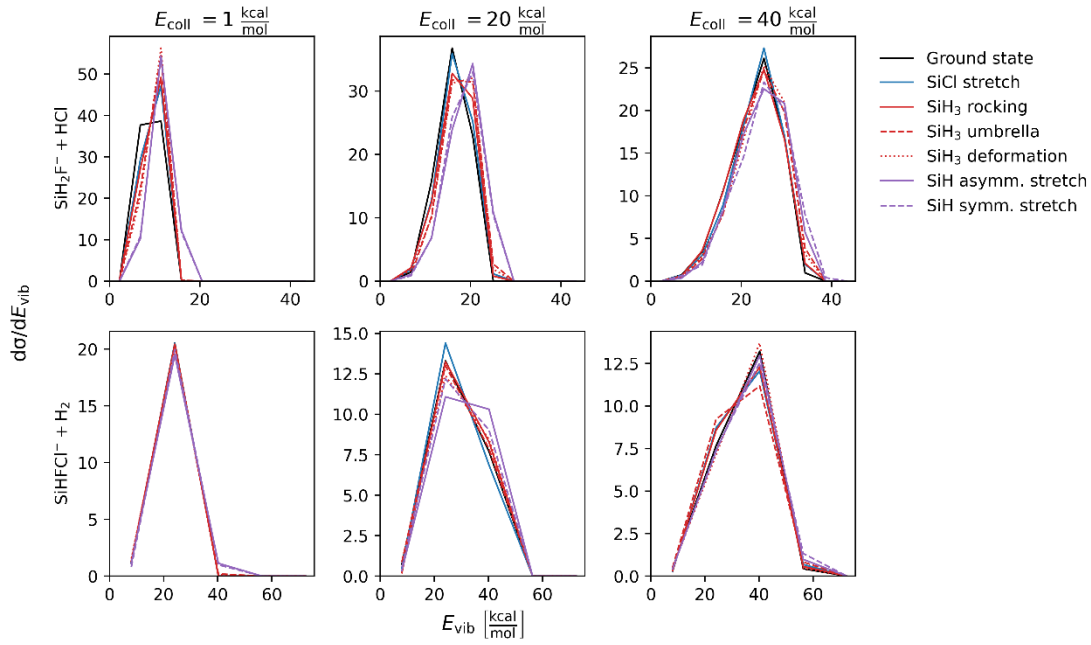

Figure S19. Mode-specific vibrational energy distributions of the F^- + $SiH_3Cl(v_k = 0, 1)$ hydrogen-chloride and molecular-hydrogen production reactions at E_{coll} = 1, 20 and 40 kcal/mol.

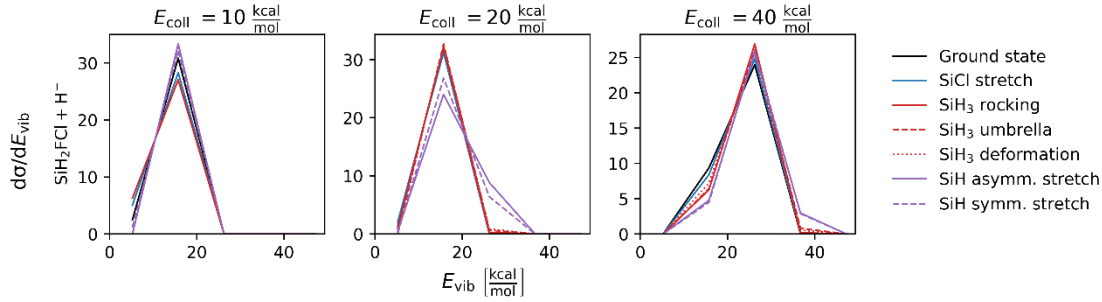

Figure S20. Mode-specific vibrational energy distributions of the F^- + $SiH_3Cl(v_k = 0, 1)$ hydride-ion substitution at E_{coll} = 10, 20 and 40 kcal/mol.

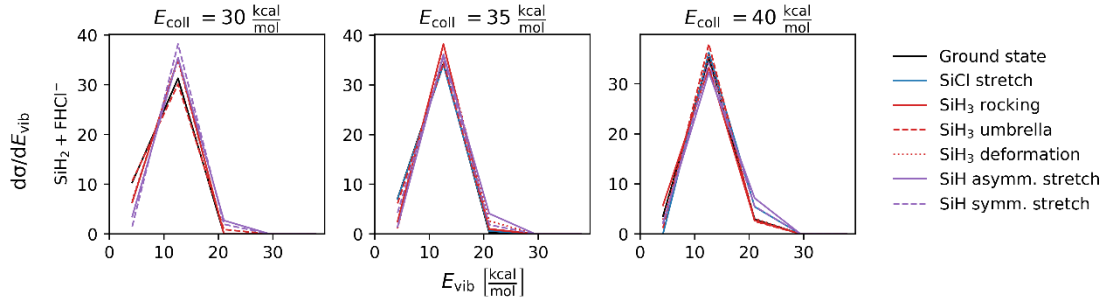

Figure S21. Mode-specific vibrational energy distributions of the F^- + $SiH_3Cl(v_k = 0, 1)$ bihalide-ion production reaction at E_{coll} = 30, 35 and 40 kcal/mol.

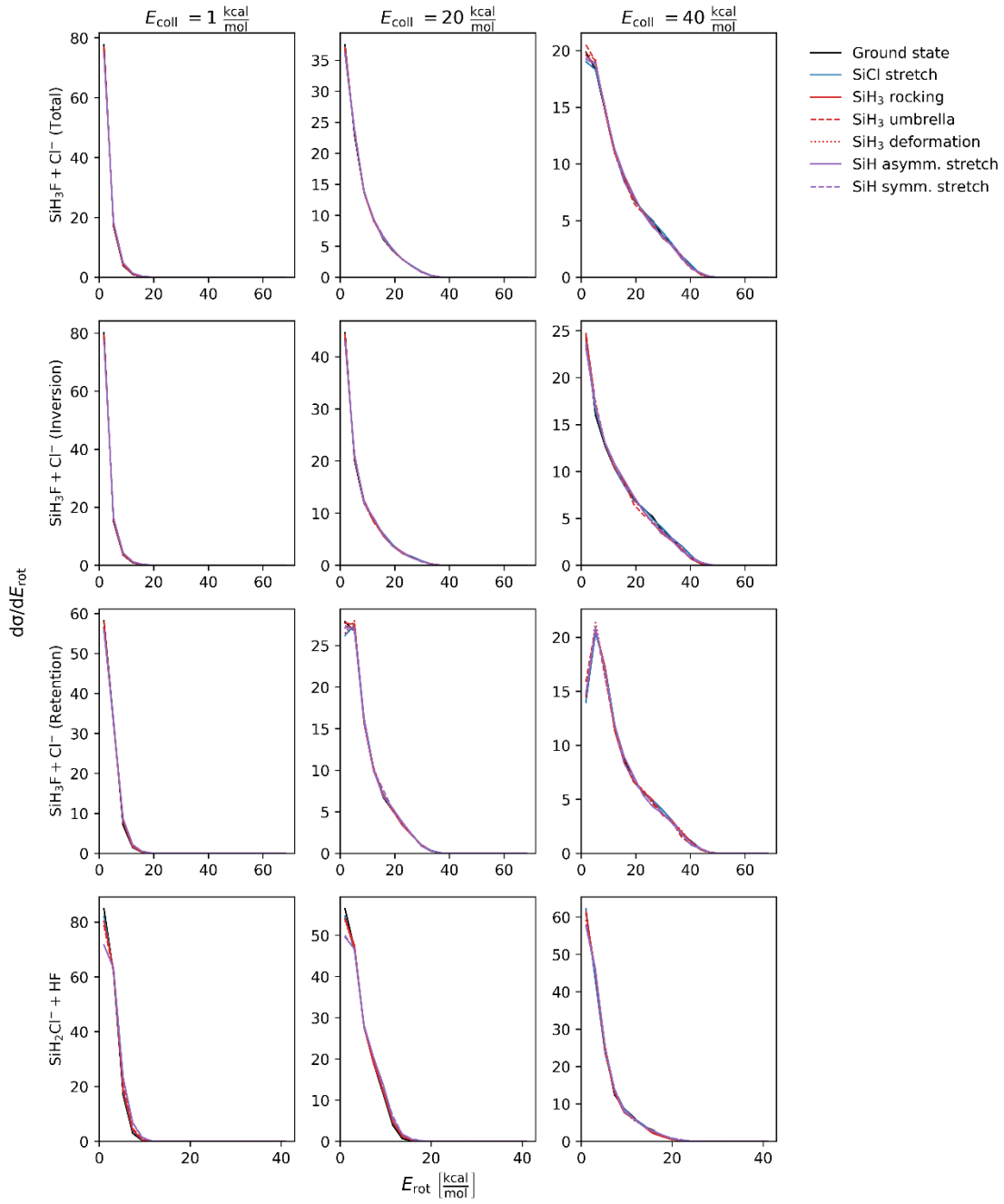

Figure S22. Mode-specific rotational energy distributions of the F^- + $SiH_3Cl(v_k = 0, 1)$ chloride-ion substitution (divided into inversion and retention channels) and proton-abstraction reactions at E_{coll} = 1, 20 and 40 kcal/mol.

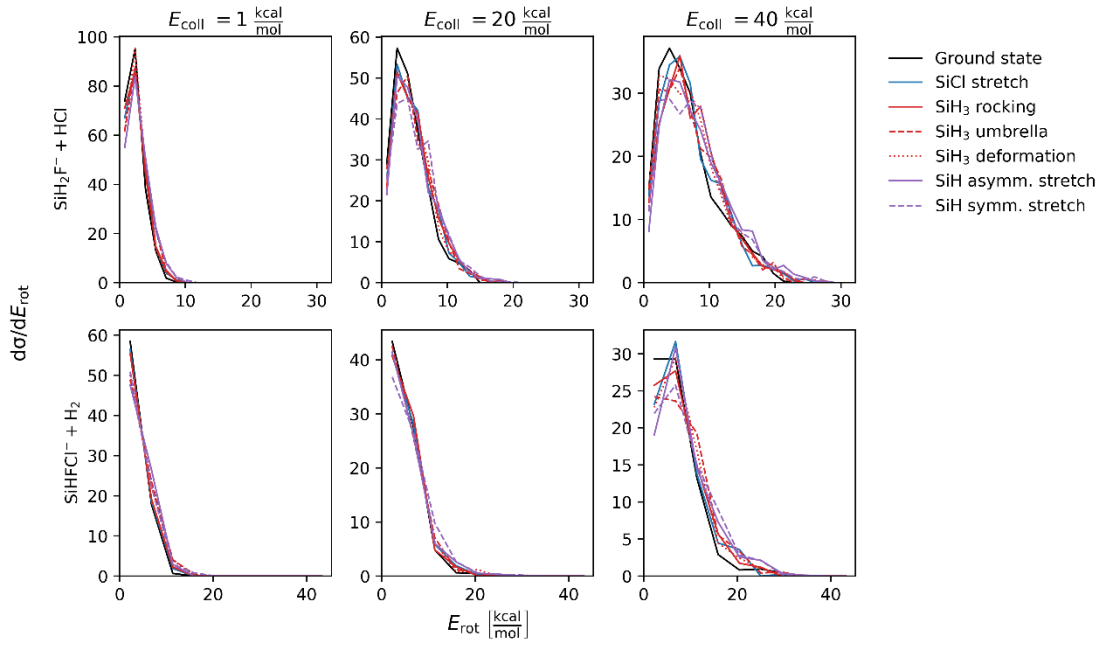

Figure S23. Mode-specific rotational energy distributions of the F^- + $SiH_3Cl(v_k = 0, 1)$ hydrogen-chloride and molecular-hydrogen production reactions at E_{coll} = 1, 20 and 40 kcal/mol.

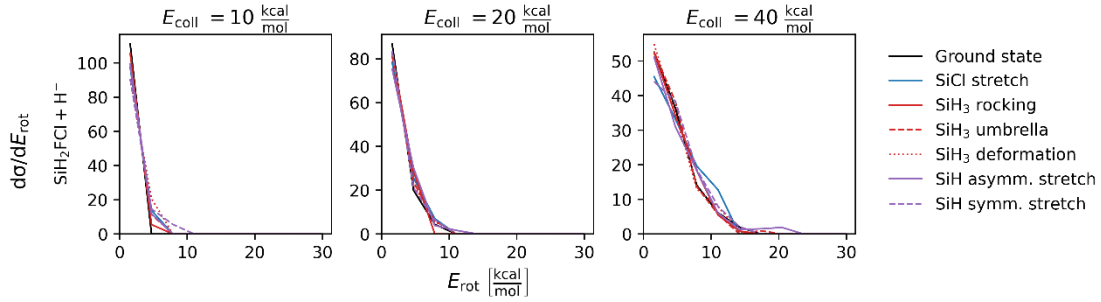

Figure S24. Mode-specific rotational energy distributions of the F^- + $SiH_3Cl(v_k = 0, 1)$ hydride-ion substitution at E_{coll} = 10, 20 and 40 kcal/mol.

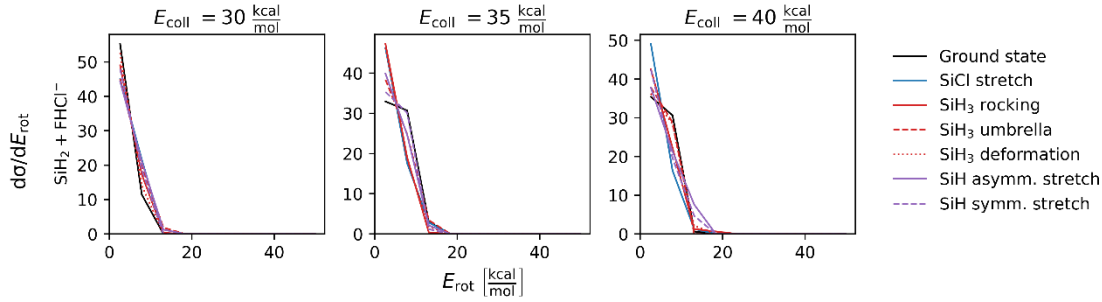

Figure S25. Mode-specific rotational energy distributions of the F^- + $SiH_3Cl(v_k = 0, 1)$ bihalide-ion production reaction at E_{coll} = 30, 35 and 40 kcal/mol.